Anal Bioanal Chem (2010) 398:3127–3138
DOI 10.1007/s00216-010-4250-2

ORIGINAL PAPER

Simultaneous determination of copper, mercury and zinc in water with a tailored fluorescent bipyridine ligand entrapped in silica sol-gel

Silvia C. Lopes Pinheiro · Ivo M. Raimundo Jr · María C. Moreno-Bondi · Guillermo Orellana

Received: 8 August 2010 / Revised: 21 September 2010 / Accepted: 22 September 2010 / Published online: 9 October 2010

Abstract A novel fluorescent ligand, (4-[(*E*)-2-(4′-methyl-2,2′-bipyridin-4-yl)vinyl]phenol) (abbreviated BSOH), has been designed and prepared for simultaneous determination of heavy metals in water. Its photophysical and photochemical properties in the absence and in the presence of Cd(II), Cu(II), Hg(II), Ni(II) and Zn(II) were determined, and the respective complexation constants (7.4×10^{3}–2.8×10^{8} l mol^{-1}) and stoichiometries were extracted thereof. The Stern–Volmer emission intensity and lifetime plots indicate an efficient static quenching of the indicator dye with the heavy metals. The BSOH fluorescent reagent has been successfully immobilised in a silica sol-gel matrix for automation of the analytical method, and the sensing phase demonstrated a reversible response to Cu(II), Hg(II) and Zn(II) but not to Cd(II) and Ni (II). Characterisation of the sensor showed that its response to those heavy metals is linear in the 2.5 to 50 μmol l^{-1} range, with a response time (t_{90}) on the order of 100 min, providing detection limits of 9.0×10^{-7}, 4.7×10^{-7} and 2.9×10^{-7} mol l^{-1} for Zn(II), Cu(II) and Hg(II), respectively. Due to the stability of the immobilised ligand, which presented no leaching from the sol-gel matrix, the simultaneous determination of the three cations in water was feasible by employing multivariate calibration techniques coupled to fluorescence quenching measurements. The sensor was validated with recovery tests by addition of Cu(II) and Hg(II) ions to spring waters, providing results with standard errors lower than 4.1 μmol l^{-1}.

Keywords Optical sensors · Fluorescence · Heavy metals · Multivariate calibration

Electronic supplementary material The online version of this article (doi:10.1007/s00216-010-4250-2) contains supplementary material, which is available to authorized users.

S. C. Lopes Pinheiro · I. M. Raimundo Jr (✉)
Institute of Chemistry, University of Campinas,
P.O. Box 6154, 13083-970 Campinas, Brazil
e-mail: ivo@iqm.unicamp.br

S. C. Lopes Pinheiro · M. C. Moreno-Bondi · G. Orellana (✉)
Optical Chemosensors and Applied Photochemistry Group (GSOLFA), Faculty of Chemistry,
Universidad Complutense de Madrid,
28040 Madrid, Spain
e-mail: orellana@quim.ucm.es

Introduction

The occurrence of heavy metal ions in waters, soils and sediments is negatively impacted by human activities such as industrialisation and the input of contaminated sewage into rivers and lakes [1]. Several heavy metal ions are very toxic to the environment and to human beings, even in low concentrations [2], while others are essential in low concentrations but hazardous in higher concentrations. Among the latter, copper(II) and zinc(II) can be mentioned due to their significance to the living organisms' metabolism, while among the former mercury(II) also plays an important role due to its high toxicity.

As a consequence of their toxicity and risks to the environment and human health, the development of analytical methods for their determination has been plentiful. Atomic absorption spectrometry, inductively coupled plasma optical emission spectrometry, inductively coupled plasma mass spectrometry and X-ray fluorescence are among the most employed techniques for *laboratory* determination of heavy metals in water. Although well established and extremely useful, these techniques present some disadvantages such as their high cost, large size of the associated instruments and impossibility of deploying them for online in situ measurements in relevant matrices [3]. Only electrochemical (such as stripping voltammetry)

or spectrophotometric methods are devoid of those limitations.

An alternative to the determination of heavy metals by conventional techniques is the development of chemical sensors or miniaturised analytical devices capable of delivering real-time online information on the presence of specific chemical species in complex samples [4]. Among the different types of chemical sensors, optical devices are widespread due to their inherent advantages of selectivity, ease of miniaturisation and robustness. Optical chemosensors applied to the determination of heavy metals based on absorbance [5, 6], reflectance [2, 7, 8] and fluorescence [9–11] measurements have been reported. Regardless of the sensing principle employed, the robustness of the indicator layer is essential for obtaining satisfactory results. As a general rule, the immobilised reagent cannot significantly leach out from the solid support but must be accessible to the target analyte. For metal ion determinations, various strategies have been employed for immobilisation of the indicator dye using poly(vinyl chloride) films [12, 13], cellulose [14, 15], Nafion [16], cross-linked acrylates [17], silica nanotubes [18] and sol-gel materials [19, 20] as supports.

The well-established sol-gel process leads to materials with capacity for reagent encapsulation and useful properties for optical sensing [21]. In general, a metal or non-metal alkoxide such as tetramethoxysilane (TMOS) or tetraethoxysilane is mixed with a co-solvent (ethanol or methanol) and water to yield a homogeneous sol. In this process, hydrolysis and condensation reactions occur, which can be accelerated with the use of appropriate acidic or basic catalysts. As the reaction progresses, the viscosity of the sol gradually increases until formation of a rigid and porous material. After ageing and drying steps, which may be carried out at ambient temperature, a xerogel is obtained. The physicochemical properties of the gel depend on the process parameters, which are controlled to yield a final material with desired features. The precursor type, pH, nature and concentration of the catalyst, water/alkoxide ratio and co-solvent(s) determine the sol-gel characteristics such as porosity, surface area, refractive index and mechanical properties. The mild reaction conditions, together with their thermal and mechanical stability and transparency in the UV-VIS, make these materials suitable for immobilising indicator molecules. Moreover, sol-gels can be obtained in different shapes and configurations, such as thin films, fibres, monoliths and powders [21–24].

Different fluorescent reagents, such as calcein [25], rhodamine [25] and *N*,*N*,*N*′,*N*′-tetrakis(2-pyridylmethyl) ethylenediamine [26], have been used for the determination of heavy metals to exploit the intrinsic sensitivity of luminescence spectroscopy. However, these reporters display poor selectivity to the analyte. As a means of circumventing this disadvantage, two main strategies have been adopted for the development of optical sensors. The first one is the synthesis of new reagents with specific structural characteristics to selectively react with a target metal ion. Eichen et al. [27] prepared the reagent 3-(3-ethoxymethyl-1*H*-imidazol-2-yl)-3-(1-ethoxymethyl-1*H*-imidazol-2-yl)-3*H*-benzo[d,e]isochromen-1-one that is selective to Zn(II), whose metal–ligand complex presents a fluorescence signal approximately 900 times more intense than that of the free ligand. Macrocyclic compounds such as calixarenes have been also used in the synthesis of complexing reagents for metal ions. Varma et al. [28] modified the calix[4]-*aza*-crown complexing agent with dansyl chloride, producing the fluorescent reagent dansyl amide-armed calix[4]-*aza*-crown, whose selectivity to Hg(II) is approximately 50 times higher than to other metal ions. A thiacalix[4]arene derivative in a 1,3-alternate conformation, bearing four quinolinoloxy groups through propyl chains, was synthesised and showed remarkable selectivity for Hg(II). Based on the fact that lumazine derivatives have been employed as a tool for the construction of functional ligands for cation recognition, Saleh [29] proposed a receptor containing the 6-thienyllumazine moiety. Preliminary studies carried out in solution showed that Cd(II) increases the fluorescence intensity, while Hg(II) and Ag(I) cause suppression of the signal. Bastida et al. [30] synthesised macrocyclic ligands holding 8-hydroxyquinoline units able to recognise heavy metals. Solution studies indicate that these ligands can be applied to the development of fluorescent sensors for the determination of Cd(II), Cu(II) and Zn(II). Duan et al. [31] have described a "turn-on"-type fluorescent sensor for Hg(II) detection. The coordination compound Cu-NB (H_2NB = bis(2-hydroxyl-naphthalene-carboxaldehyde) benzyldihydrazone) exhibits low fluorescence due to the presence of Cu(II) ("off" state). After the addition of Hg(II), Cu(II) ions are displaced from the complex, yielding a product whose fluorescence is more intense ("on" state). The coordination of Cu(II) in the ligand structure avoids cross-sensitivity of other cations, making the reagent selective to Hg(II).

As the design and preparation of a highly selective molecular sensor are difficult tasks, a second strategy to overcome the lack of reagent selectivity for multiple metal ion analysis is the use of multivariate calibration techniques [32]. Among the methods of multivariate calibration for the simultaneous determination of metal ions, principal component regression (PCR) [32, 33], artificial neural networks [8, 34, 35] and partial least square (PLS) [32, 33] have been successfully used. These methods have been applied to spectroscopic analysis due to their ability to deal with problems regarding spectral data collinearity and absorption band overlap. Although such tools have been extensively employed for simultaneous determination of multiple species in solution [32–35], their application to optical sensors is still scarce, mainly due to the stability of the sensing phase. As a multivariate calibration requires a large number of measurements, leaching of the immobilised reagent, even at a low rate,

produces inconsistent spectral data in which variability does not only represent the differences among the calibration/sample solutions but also the change in the amount of polymer-supported indicator. In addition, sensors based on fluorescence quenching bring about an extra challenge, as the emission spectrum is due to the free ligand and, therefore, the same for all metal–ligand complexes formed. In this case, differentiation between signals due to distinct metal ions can arise as a consequence of the reaction kinetics or mass transfer rate of the analytes from the solution to the sensing layer [8] as well as some disturbance that the interactions with specific metal ions cause to the free ligand.

The usefulness and importance of 2,2′-bipyridine and 1,10-phenanthroline in chemical analysis have been put forward in most textbooks. Colourimetric or fluorometric determination of many metal ions is based on the coordination compounds formed in solution by those chelating ligands and most metal ions (including rare earths) in the Periodic Table [36]. Therefore, bipyridine and phenanthroline are the paradigm of intrinsically *unselective* ligands, yet specific metal ions can be analysed if adequately substituted derivatives are prepared due to the different coordination number and geometry of the former [36]. Cu(II) salts yield a variety of complex species depending on the metal-to-ligand ratio and the conditions employed. Bipyridine binds Cu(II) in a 1:1 ratio with K_a of 2.95×10^8 l mol^{-1}. A similar constant has been measured for Hg(II) (4.36×10^9 l mol^{-1}), but Zn(II) displays a much lower affinity for this ligand (1.44×10^5 l mol^{-1}) [37]. Interestingly enough, Zn(II) has also the lowest rate constant of adduct formation of the three investigated metal ions (10^6 vs. $\geq10^7$ l mol^{-1} s^{-1}) [36].

The aim of this is work has been the design, preparation and characterisation of a new fluorescent reagent for the simultaneous determination of copper, mercury and zinc ions in water. The 2,2′-bipyridine ligand seemed to be an appropriate starting point for complexation to a variety of metal ions; however, bipyridines are non-fluorescent so that tailored functionalisation was essential to achieve a fluorescent molecular sensor for high sensitivity. With the aim of using silica sol-gel materials to immobilise the indicator dye, the presence of a hydroxyl group in the latter was deemed essential for the attachment of the fluorescent molecular sensor to the sol-gel network during the polymerisation process. Obviously, attachment to the indicator to its solid support is advantageous to avoid leaching and increase the operational lifetime of the sensor layer but should not affect its optical properties. With such a molecular design in mind, the novel fluorescent ligand BSOH (Fig. 1) was prepared and evaluated regarding its complexing ability for metal ions in connection to its spectroscopic properties. Once its fitness to purpose was assessed, BSOH has been immobilised in a sol-gel matrix and its reversible response to Cu(II), Hg(II) and Zn(II) was evaluated.

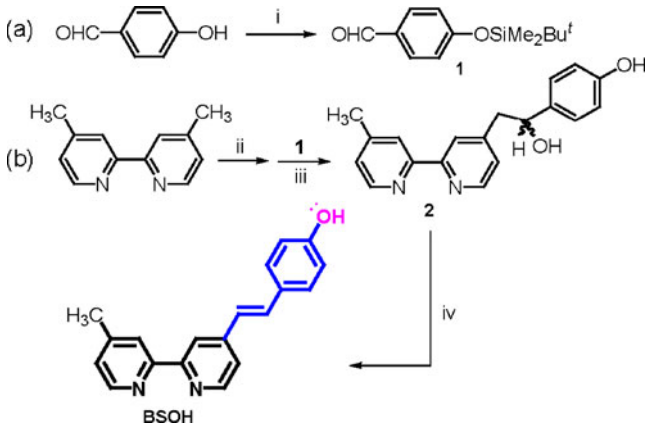

Fig. 1 Reagents and conditions: (*i*) *t*-butyldimethylsilyl chloride/DBU/acetonitrile/Ar/room temp.; (*ii*) lithium diisopropylamide/THF/Ar/−78 °C; (*iii*) THF/−78 °C/1 h; then room temp./12 h followed by hydrolysis; (*iv*) *p*-toluene sulphonic acid/Ar/70 °C/20 h. The metal ion complexing and fluorophoric and chemically reactive moieties of BSOH have been emphasised (see text)

The sensor phase has been employed to simultaneously determine those ions in water using multivariate-calibration-based on PLS regression and fluorescence quenching, which would not be feasible in solution as the analytical signals comes from the free ligand and would be the same regardless the kind of metal ion.

Experimental

Synthesis of the fluorescent indicator dye

The chelating ligand BSOH was prepared from commercial 4,4′-dimethyl-2,2′-bipyridine and 4-hydroxybenzaldehyde (Fig. 1). (a) A mixture of 1.0 g (8.19 mmol) of *p*-hydroxybenzaldehyde (98%, Aldrich) and 1.51 g (10.02 mmol) of *t*-butyldimethylsilyl chloride (97%, Fluka) is dissolved in 10 ml of anhydrous acetonitrile (Fluka). After introducing argon for 20 min in the reaction flask, 1.6 ml (10.65 mmol) of 1,8-diazabicyclo[5.4.0]undec-7-ene (DBU, 98%, Aldrich) in 5 ml of anhydrous acetonitrile is added, and the reaction mixture is stirred at room temperature. After checking that the starting aldehyde has been consumed (approximately 2 h), the solvent is evaporated under reduced pressure, and the resulting yellow oil is subject to vacuum distillation (126 °C, 3 Torr) to yield the pure colourless *O*-silyl derivative (**1**) in 50% yield. (b) A solution of lithium diisopropylamide (2.6 mmol, Aldrich) in 4 ml of anhydrous tetrahydrofuran (THF) (Fluka) is cooled to −78 °C while argon is being introduced in the flask. Then a solution of 4,4′-dimethyl-2,2′-bipyridine (2.6 mmol, Aldrich) in 25 ml of anhydrous THF is added dropwise to the reaction flask. Formation of the dimethyl bipyridine carbanion is signalled by the appearance of an

intense dark red colour. After 2 h of stirring at −78 °C, 3.15 mmol of the benzaldehyde derivative **1** dissolved in 4 ml of anhydrous THF is added. The cooling bath is removed, and the reaction is left to evolve at room temperature for 14 h. Then 5 g of ice is added to the reaction mixture; the solvent is evaporated at reduced pressure, and the sought alcohol (**2**) is isolated as a yellow solid by suspension of the residue in methanol/chloroform. (c) The arylhydroxymethylbipyridine **2** (0.60 g, 1.96 mmol) is dissolved in 10 ml of anhydrous toluene (Fluka), and argon is introduced into the reaction flask. Then 0.255 g of *p*-toluene sulphonic acid (Panreac, purified by recrystallisation from ethyl acetate) in 10 ml of anhydrous toluene is added. The resulting yellow suspension is heated to 70 °C and left to react for 24 h. The original yellow solid dissolves, and a red precipitate appears over time. The solid is filtered out, dissolved in methanol and re-precipitated with acetonitrile to yield 0.51 g of BSOH (90% yield). The product structure is confirmed by its 500-MHz ^{1}H-nuclear magnetic resonance (NMR) data in methanol-d_4 (see Fig. S1 in the Electronic Supplementary Material).

Analytical reagents and apparatus

Analytical-grade reagents from Sigma-Aldrich Quimica (Madrid, Spain) and water purified with a Millipore Direct-Q system (Millipore, Bedford, MA, USA) were used throughout. Buffer solutions (0.1 mol l^{-1}) in the pH 2.0 to 12.0 range were prepared from dipotassium hydrogen phosphate, potassium dihydrogen phosphate, potassium phosphate and hydrochloric acid or sodium hydroxide solutions. Anhydrous methanol (over molecular sieves) was from Fluka. Stock solutions of the different metals were prepared in methanol from mercury chloride ($HgCl_2$), zinc chloride ($ZnCl_2$), copper sulphate pentahydrate ($CuSO_4{\cdot}5H_2O$), nickel chloride hexahydrate ($NiCl_2{\cdot}6H_2O$) and cadmium nitrate tetrahydrate ($Cd(NO_3)_2{\cdot}4H_2O$) obtained from Vetec (São Paulo, Brazil). Lower concentrations were prepared by serial dilutions of the stock with phosphate buffer of adequate pH.

The pH of samples and buffer solutions was adjusted with a Corning 443i pH metre (São Paulo, Brazil) equipped with a combination glass electrode. The 500-MHz ^{1}H-NMR spectra have been obtained at UCM Central NMR Instrumentation Facilities with a Bruker AVANCE AV-500 spectrometer. Surface area of the sol-gel material was determined with an Autosorb I from Quantachrome Instruments (Boynton Beach, FL, USA). UV-VIS absorption spectra were recorded using a Varian Cary 3-Bio (Palo Alto, CA, USA). The metal–ligand equilibrium constants and stoichiometry of the corresponding complexes were determined with Hyperquad 2006 software (Protonic Software, www.hyperquad.co.uk). Hyperquad is a computer programme which provides (1) a system for simulating titration curves and (2) a system for providing speciation diagrams. The calculations relate to equilibria in solution; there are no restrictions as to the number of species that may be present or the number of complexes that may be formed. Fluorescence data from solutions were collected using a Perkin-Elmer LS50B spectrofluorometer (Sussex, UK), setting slit widths at 6 nm. A Varian Cary Eclipse fluorescence spectrometer was employed for measurements with the sol-gel sensing phase, adopting slit widths of 10 nm and a 430-nm cutoff filter in the emission path. Emission lifetime measurements were carried out using a Horiba Jobin Yvon Fluoromax-4TCSPC spectrofluorometer (New Jersey, USA) equipped with a Horiba NanoLed-370 laser diode (700-ps 370-nm pulses at 500 kHz). Fluorescence decays were measured with a 200-ns window (4,096 channels) by accumulating 10,000 counts in the peak channel, and emission lifetimes were extracted from the exponential curve fittings using the proprietary H-J-Y hybrid grid-search minimisation algorithm (without deconvolution) for stable chi-squared minimisation. Any observed decay component equal to or below the laser pulse width was discarded.

Sol-gel preparation and instrumental setup

The sol-gel sensing phases were prepared by mixing 5.0 ml of TMOS (99%, Aldrich), 6.0 ml of methanol (J.T. Baker) and 2.4 ml of water in a beaker. The mixture was stirred for 5 min followed by the addition of a solution containing 1.38 mg of BSOH and 250 μl of 1.30×10^{-6} mol l^{-1} NH_4OH (Aldrich) in 9.0 ml of methanol. The sols were allowed to gel and dry at room temperature to constant weight for approximately 20 days. The resulting sol-gel was mechanically crushed and sieved, and the 100–150-μm sol-gel particles were packed in a 100-μl 3-mm path fluorescence flow-through quartz cell (Hellma, Germany) for the metal ion analysis. At the top of the cell chamber, a small nylon mesh plug was placed to prevent particle displacement by the flow stream.

The flow-through cell was placed in the spectrofluorometer sample holder. The sample flow stream was generated by a peristaltic pump (Ismatec IPC 8, Switzerland). The carrier solution consisted of pH 5.0 phosphate buffer that was pumped for 20 min through the sensing phase at a constant flow rate of 0.3 ml min^{-1}. Once a stable baseline was obtained, 3.00 ml (10 min) of the heavy metal sample solution was pumped through the system and the decrease of the fluorescence signal was evaluated. Finally, the sensing phase was regenerated with 550 μl (2 min) of 0.1 mol l^{-1} HCl, and buffer solution was pumped through the flow cell, in order to obtain the reference signal. All determinations were carried out in triplicate.

Multivariate calibration

For the simultaneous determination of the metal ions, binary and ternary mixtures were prepared according to a

central composite design. A concentration range from 2.50 to 50.0 μmol l^{-1} was employed for all species. The excitation wavelength was set at 410 nm, and emission spectra from 420 to 650 nm were acquired every 2 min for a total time interval of 10 min. The multivariate calibration models were constructed by employing the I_0/I_i spectral ratio, where I_0 is the reference spectrum (obtained in buffer solution) and I_i is the fluorescence spectrum obtained by pumping sample solution through the flow cell after i min (i= 2, 4, 6, 8 and 10 min). The I_0/I_i spectral data were submitted to different smoothing pre-treatments, based on moving average, median filter and Savitzky–Golay filter (with various different windows), aimed at improving the signal-to-noise ratio of the data. *Unscrambler 9.7* (CAMO) and *MatLab 6.5* (MathWorks) software were employed for the construction of the PLS calibration models, which were based on PLS regression.

Results and discussion

Characterisation of the BSOH ligand in methanol

The chemical structure of the novel BSOH ligand is shown in Fig. 1. The BSOH structure depicts the three distinct functional moieties sought in the molecular design of an optimum fluorescent indicator for unspecific heavy metal ion analysis to be incorporated into a sol-gel matrix. The *E* configuration of the stilbene moiety is evidenced by the $^3J_{H\text{-}H}$ coupling constant measured in the NMR spectrum (16.5 Hz). Since the last step of the synthesis of BSOH involves thermal dehydration of the precursor alcohol in the presence of a strong acid, predominant formation of the thermodynamically most stable product is warranted. Nevertheless, approximately 15% of the *Z* stilbene isomer is also obtained, as deduced from the ^{1}H-NMR spectrum of the product. No attempt to separate the diastereoisomers was made.

The stilbene feature is associated with intense absorption and fluorescent properties [38]. Due to its scarce solubility in water, the spectroscopic features of the BSOH ligand were characterised firstly in methanol solution. Figure 2 shows its absorption spectrum recorded in this solvent. It can be observed that the free ligand presents three absorption bands, centred at 235, 282 and 336 nm. At the latter wavelength, the molar absorption coefficient at 25 °C is 1.29×10^4 l mol^{-1} cm^{-1}. Figure 2 also depicts the excitation and emission spectra, demonstrating that the wavelength of maximum absorbance at lowest energy coincides with that of the excitation peak. The fluorescence peak occurs at 440 nm in methanol, significantly red-shifted compared to the Stokes shift of stilbene [38] due to the intramolecular charge transfer (ICT) nature of the emissive state of BSOH in polar solvents.

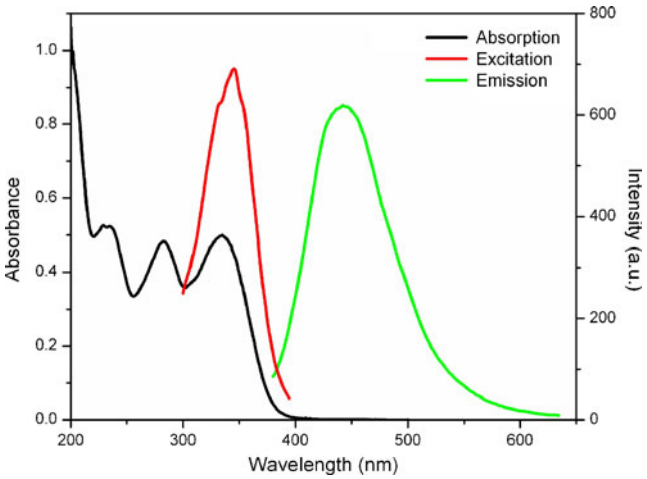

Fig. 2 Electronic absorption, excitation and emission spectra of BSOH (3.61×10^{-5} mol l^{-1}) in methanol (excitation at 336 nm and emission at 440 nm)

Complexation of BSOH with different heavy metal ions of interest, namely Cd(II), Cu(II), Hg(II), Ni(II) and Zn(II), was screened in methanol by employing 5.13×10^{-5} mol l^{-1} solutions of the molecular reporter containing each of them 1.0×10^{-4} mol l^{-1} of the investigated metal ion. It can be observed from Fig. 3 that the absorption spectra of the metal–ligand complexes are all different, always displaying a bathochromic shift, the extension of which depends on the heavy metal ion. Different profiles and intensities are also observed for the emission spectra of BSOH in the presence of the selected metal ions, as illustrated in Fig. 4. Cd(II) and Hg(II) slightly enhance the fluorescence of the ligand, while Zn(II), Cu(II) and Ni(II) act as fluorescence quenchers (the last two ions have a dramatic effect, as the emission intensity reaches a value close to zero). These differences found in both types of spectra make BSOH a very appropriate ligand for simultaneous determination of metal ions.

According to the different ease of reduction of the investigated metal ions, a photo-induced electron transfer (PET) from the phenolic bipyridine BSOH ligand to the coordinated metal ion would be expected, particularly efficient for Hg(II), Cu(II) and Ni(II) (i.e. the easiest to reduce ions). Surprisingly, coordination to Hg(II) does not lead to fluorescence quenching in solution. In the absence of a more detailed photochemical study (far from the aim of this paper), we speculate that under the experimental conditions of Fig. 4 the reducing phenol moiety of the BSOH fluorophore is fully coordinated to Hg(II), efficiently preventing the PET deactivation mechanism. Coordination of the phenol group to the other metal ions would be less favourable, and chelation by the bipyridine moiety would prevail. Recovery of the PET quenching of the fluorophore upon immobilisation into the sol-gel (see below) lends further support to this hypothesis.

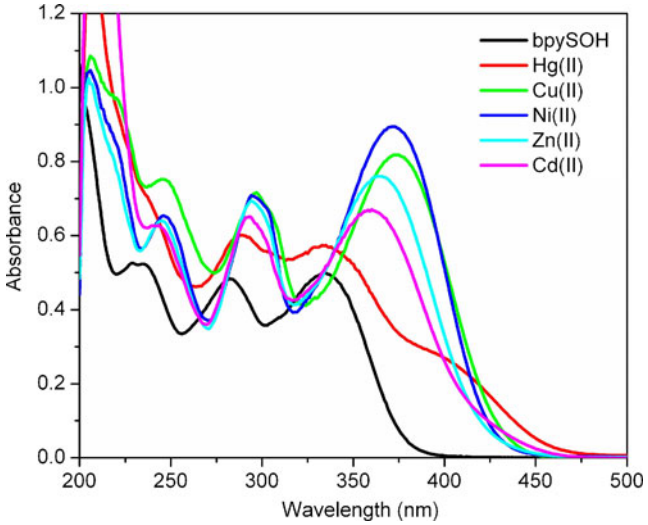

Fig. 3 Absorption spectra of BSOH (5.13×10^{-5} mol l^{-1}) in methanol in the absence and in the presence of 1.02×10^{-4} mol l^{-1} of Cd(II), 1.03×10^{-4} mol l^{-1} of Cu(II), 1.09×10^{-4} mol l^{-1} of Hg(II), 1.04×10^{-4} mol l^{-1} of Ni(II) and 1.02×10^{-4} mol l^{-1} of Zn(II)

The stoichiometry of the complexes formed between the ligand and each of the investigated metal ions was determined by the molar ratio method, in which the ligand absorption spectra are evaluated as a function of the metal ion concentration for a fixed host concentration. In addition, the stability constants were calculated from those spectra with the aid of the Hyperquad software v.2006 (Protonic Software). Table 1 summarises the results obtained, showing that the metal–ligand complexes formed with Cu(II), Hg(II) and Zn(II) are much more stable than those with Ni(II) and Cd(II). Moreover, in spite of their low association constant with BSOH, these last two ions bind

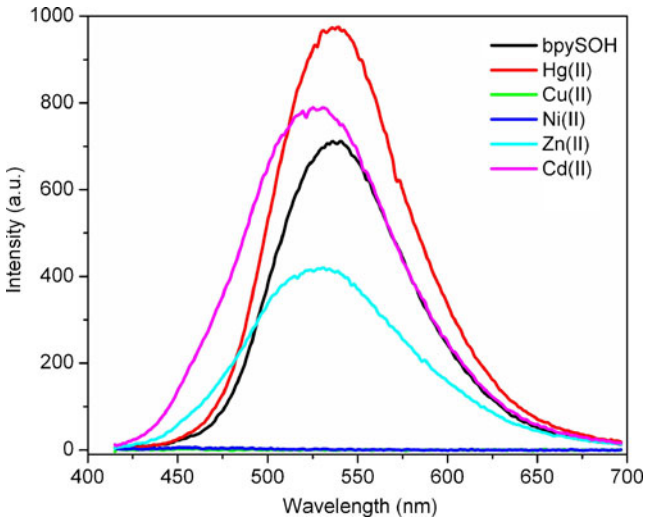

Fig. 4 Fluorescence spectra of BSOH (5.13×10^{-5} mol l^{-1}) in methanol in the absence and in the presence of 1.02×10^{-4} mol l^{-1} of Cd(II), 1.03×10^{-4} mol l^{-1} of Cu(II), 1.09×10^{-4} mol l^{-1} of Hg(II), 1.04×10^{-4} mol l^{-1} of Ni(II) and 1.02×10^{-4} mol l^{-1} of Zn(II). All the spectra have been recorded with excitation at 336 nm

Table 1 Determined stoichiometry and overall association constants of the metal ion–BSOH complexes in methanol (BSOH=3.0×10^{-5} mol l^{-1})

Metal	BSOH:M(II)	K (l mol^{-1})
Cd(II)	1:1	7.44×10^{3}
Cu(II)	2:1	2.79×10^{8}
Hg(II)	2:1	1.98×10^{7}
Ni(II)	1:1	1.21×10^{4}
Zn(II)	1:1	3.88×10^{7}

irreversibly with the ligand when it is immobilised in a sol-gel matrix, as will be discussed later. Due to these facts, further photophysical studies focused only on Cu(II), Hg(II) and Zn (II) ions.

Solutions with different BSOH concentrations were prepared in methanol, and the fluorescence lifetime values of the indicator dye were measured. A lifetime of 3.8± 0.2 ns was obtained regardless the ligand concentration or the presence of dissolved oxygen, a result that is compatible with the ICT nature of the emissive excited state (the excited state lifetime of stilbenes without conjugated donor/acceptor groups attached to the aromatic system is typically below 1 ns [38]). For the determination of the lifetime of metal ion complexes, a 3.92×10^{-5} mol l^{-1} BSOH solution was prepared and the fluorescence decay profiles were measured upon increasing the concentration of metal ions from 1.50×10^{-6} to 1.50×10^{-5} mol l^{-1}. As it can be seen in Table 2, the fluorescence lifetime values of BSOH (but not the emission intensity, see above) remain constant and independent of the metal ion concentration, indicating the *static* nature of the emission quenching observed upon formation of the metal–ligand adduct.

Characterisation of the BSOH ligand in water

Further UV-VIS absorption studies were carried out with BSOH (2.95×10^{-5} mol l^{-1}) in Britton–Robinson buffer

Table 2 Fluorescence lifetime of BSOH as a function of the heavy metal concentration in methanol (BSOH=3.9×10^{-5} mol l^{-1})

[M(II)] (mol l^{-1})	τ (ns)		
	+Cu(II)	+Hg(II)	+Zn(II)
0	3.67	3.65	3.98
1.50×10^{-6}	3.63	3.68	3.95
3.50×10^{-6}	3.64	3.63	3.96
7.50×10^{-6}	3.71	3.84	3.90
1.00×10^{-5}	3.69	3.76	4.05
1.50×10^{-5}	3.73	3.61	4.17

solutions, with ionic strength of 0.5 mol l^{-1} and pH interval from 2 to 12 (Fig. 5). It can be observed that the absorption band around 380 nm is practically constant up to pH 4.0, presenting a decrease up to pH 8.0, increasing again at pH values higher than 9. In addition, the absorption spectra display two isosbestic points, one just above 350 nm (occurring from pH 2.0 to 7.0) and the other just below 350 nm that appears at pH values higher than 8.0, a fact that evidences the complexity of the system under equilibrium (the BSOH molecule has two protonation and one deprotonation site, Fig. 1). Figure 6 depicts the emission spectra of the ligand as a function of pH, upon excitation at 336 nm. There are three sets of emission bands, with maximums at 523 nm (pH 2.2–4.2), 453 nm (pH 5.1–11.0) and 385 nm (pH 11.8), which are the consequence of the protonation state of the indicator molecule. A more detailed photochemical discussion

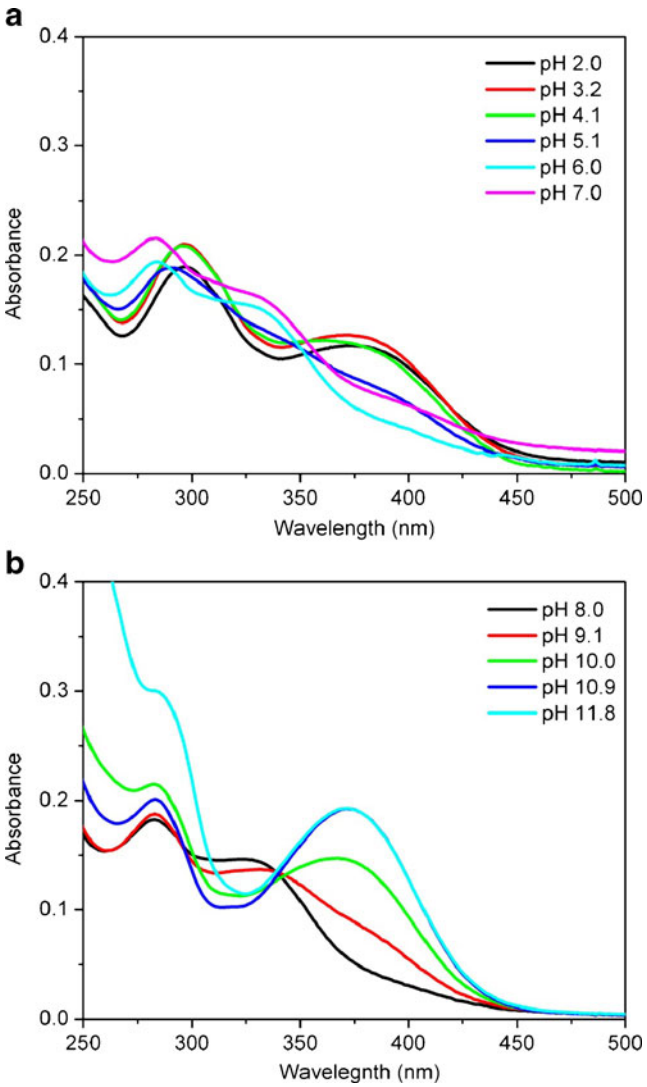

Fig. 5 Absorption spectra of BSOH (2.95×10^{-5} mol l^{-1}) in Britton–Robinson buffer solutions (ionic strength of 0.5 mol l^{-1}) in the pH intervals **a** 2.0–7.0 and **b** 8.0–11.8

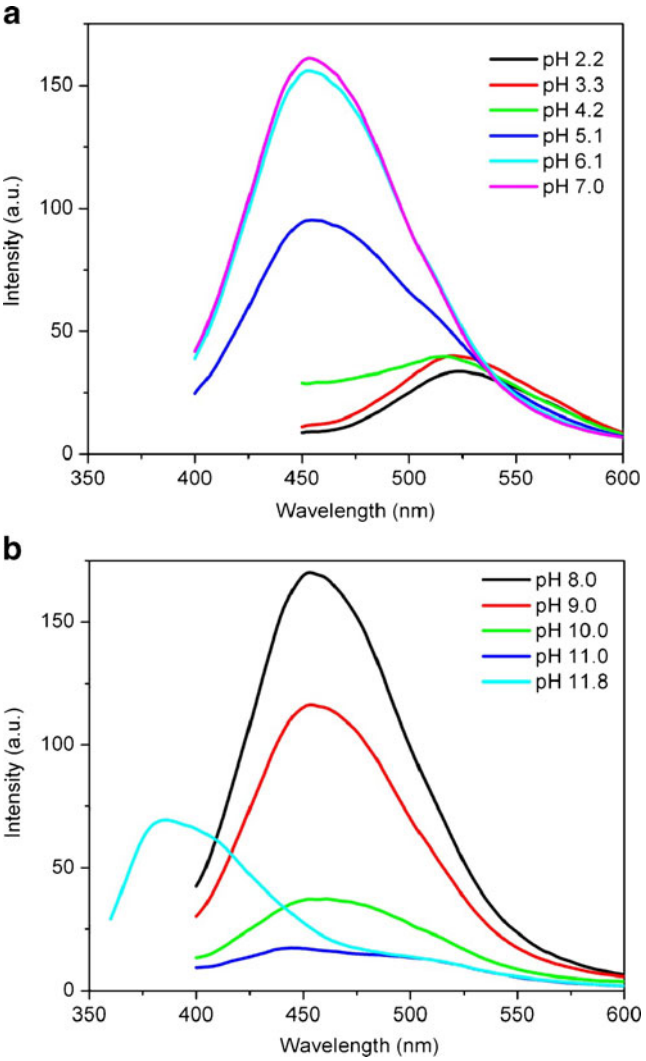

Fig. 6 Fluorescence spectra of BSOH (2.95×10^{-5} mol l^{-1}) in Britton–Robinson buffer solutions (ionic strength of 0.5 mol l^{-1}) in the pH intervals **a** 2.0–7.0 and **b** 8.0–11.8 (excitation at 336 nm)

on this issue would require more elaborate physicochemical data and is out of the scope of this work. As can be seen in Fig. 6, the most intense fluorescence is measured in the pH 6.1–8.0 range; thus, solutions buffered at pH 7.0 were employed for studying the interaction of the ligand with metal ions, as this value favours the conditional formation constants avoiding the precipitation of metal ions hydroxides.

A predictive calculation of the ionisation constants of BSOH using the ACD/p*K*a v5.0 software yields pK_a values of 9.75±0.15 and 4.88±0.37 for the deprotonation of the phenol group and the protonation of the bipyridine moiety (in the 4-methylpyridine ring), respectively. Therefore, the ligand is expected to be unprotonated (electrically neutral) in pH 7.0 buffered solution.

The formation of BSOH–metal ion complexes was evaluated in 20 mmol l^{-1} buffer solutions at pH 7.0. Absorption spectra were different for each metal ion, similar

to the results obtained in methanol solution. However, only Hg(II) produced an enhancement of fluorescence intensity, while Cu(II), Ni(II), Cd(II) and Zn(II) all quenched the fluorescence intensity (but not the BSOH emission lifetime, see Table 2). The emission spectra for all metal ions displayed a maximum at 455 nm and a linear response range from 1.50×10^{-7} to 6.00×10^{-6} mol l^{-1}, values which guided the studies with the sol-gel sensing phase.

Evaluation of the BSOH immobilised in a sol-gel matrix

The solid obtained in the sol-gel process showed a light-yellow colour even after thorough washing with methanol and other organic solvents where BSOH is very soluble, indicating the chemical immobilisation of the ligand in the matrix. Preliminary experiments demonstrated the efficient immobilisation of the ligand, as its leaching from the solid support was never observed. This observation confirms that the BSOH indicator dye is covalently tethered to the SiO_2 matrix through its –OH group, imparting a high chemical stability to the sensing phase.

The surface area (S_{BET}) of the sol-gel was determined by nitrogen adsorption based on the BET method, providing a value of 470.4 m^2 g^{-1}. A porous diameter of 17.8 Å and a porous specific volume of 0.21 cm^3 g^{-1} were obtained, characterising the sol-gel as a microporous material.

The evaluation of the excitation and emission spectra of the solid phase in pH 7.0 buffer solution revealed peaks at 410 and 515 nm, respectively, which differ from the values obtained in solution (380 and 455 nm), as a consequence of the encapsulation of the ligand in the sol-gel matrix via covalent binding by the phenol group. Figure 7 shows the emission spectra of the immobilised ligand obtained in solutions with different pH values. As it can be observed, the signal decreases as the pH increases, and no significant band shift occurs, a different behaviour from that in aqueous solution. However, the fluorescence signals obtained at pH 2.3, 3.1 and 4.1 display the same intensity, and the decrease in the fluorescence at pH 5.0 coincides with the shift observed in aqueous solutions at the same values of pH. These results may suggest that a proton attached to the nitrogen atom of the bipyridine moiety (see above) is being titrated between pH 4.0 and 5.0, a fact that is in agreement with the p*K*a calculated value of 4.88. Thus, solutions buffered at pH 5.0 were used throughout the studies because below this value protonation of the BSOH ligand impairs the complexing reaction of the metal ions.

The reaction of the immobilised ligand with the selected heavy metal ions showed an irreversible response to Cd(II) and Ni(II), as regeneration of the free ligand was not achieved even after flowing 0.10 mol l^{-1} HCl solution for a long period of time. No interference of Ca(II), Fe(III) and Pb(II) was observed at 50 μmol l^{-1}. On the other hand,

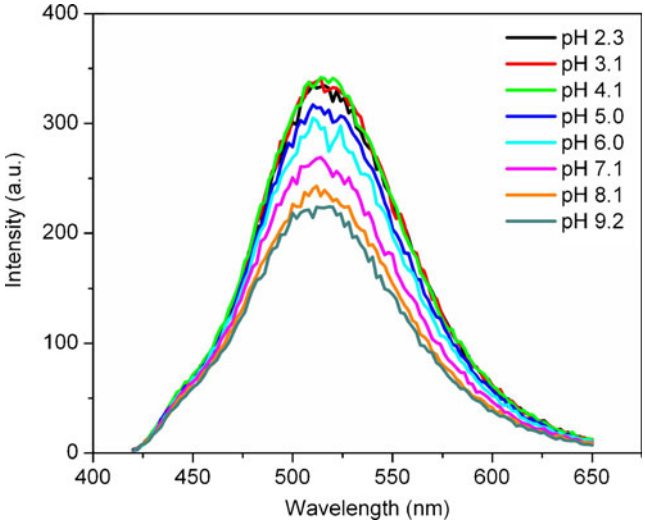

Fig. 7 Fluorescence spectra of BSOH immobilised in the sol-gel matrix obtained in Britton–Robinson buffer solutions at different pH values (excitation at 410 nm)

dissolved Zn(II), Hg(II) and Cu(II) ions tightly bound to the sensing phase cause a decrease in the fluorescence intensity, and the baseline signal had to be recovered with a 0.1 mol l^{-1} HCl solution. Remarkably enough, Hg(II) also quenched the BSOH fluorescence, unlike the behaviour observed in solution. Recovery of the expected fluorescence quenching by PET to the metal ion might be a consequence of the covalent binding of the BSOH ligand to the siloxane backbone by its phenol moiety during formation of the sol-gel. In this way, phenol coordination to the Hg(II) ion would not occur, and efficient PET from the unshared electron pair of the oxygen atom to the bpy-coordinated Hg(II) would be recovered.

Figure 8 illustrates the fluorescence signal of the sensor phase in the presence of different Hg(II) concentrations at pH 5.0, setting the excitation and emission wavelengths at 410 and 515 nm, respectively. The response curve was obtained by pumping pH 5.0 buffer solution for 20 min (I_0 signal), metal ion sample solution for 10 min and 0.1 mol l^{-1} HCl solution for an additional 2 min (regeneration of the free ligand) at a flow rate of 0.3 ml min^{-1}. As it can be observed, the repeatability of the signals is adequate (relative standard deviation lower than 3.0%) and the baseline is stable, indicating the regeneration of the free ligand. Similar curves were obtained for Cu(II) and Zn(II) ions, although with different sensitivities (Hg > Cu > Zn) following the ease of reduction of the corresponding 2+ ions. These features are important for a successful multivariate calibration. Independent of the metal ion sensitivity, under the experimental conditions employed, the sensing phase was saturated for solutions with concentrations higher than 50 μmol l^{-1} as the fluorescence signal reached a plateau value. The response

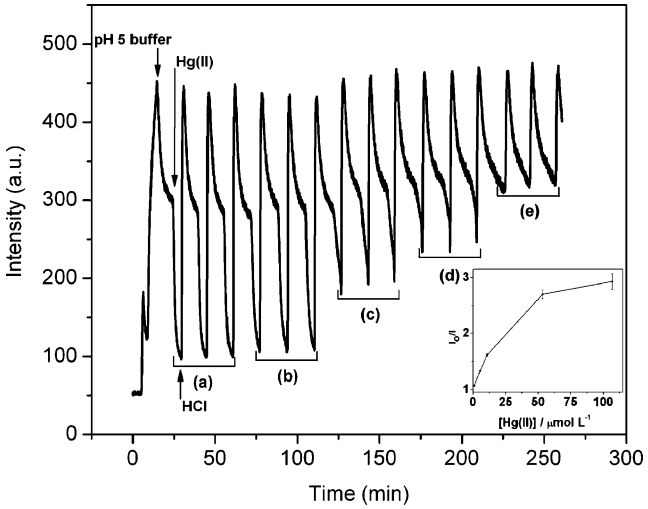

Fig. 8 Fluorescence intensity signals obtained with immobilised BSOH for Hg(II) concentrations of: (*a*) 107, (*b*) 53.5, (*c*) 10.7, (*d*) 5.35 and (*e*) 1.07 μmol l^{-1} (excitation at 410 nm and emission at 515 nm)

time ($t_{90\%}$) was determined by using 25-μmol l^{-1} solutions of the metal ions flowing at 0.3 ml min^{-1}, yielding values of 88, 107 and 114 min for Cu(II), Hg(II) and Zn(II), respectively. By performing univariate calibrations, detection limits of 8.9×10^{-7}, 4.7×10^{-7} and 2.9×10^{-7} mol l^{-1} were obtained for Zn (II), Cu(II) and Hg(II), respectively, values that are below the limits established by legislation, except for Hg(II). However, it is important to mention that these values can be further improved if the analytical signal is taken closer to the response time of the sensor and not after just 10 min of reaction, signal, at the expense of a lower sample throughput. Moreover, the sensing phase was not optimised to achieve the best limit of detection for a given metal ion but to balance the sensitivity among the species studied. By this approach, it was possible to demonstrate the feasibility of simultaneous determination of those metal ions using a covalently immobilised reagent, fluorescence quenching and multivariate calibration.

Regeneration of the free ligand was also evaluated by employing 0.10 mol l^{-1} EDTA, 0.01 mol l^{-1} H_3PO_4 solutions, which were inefficient to perform this task, and 0.01 mol l^{-1} HCl solution, which required a very long time for full regeneration of the sensitive phase.

Simultaneous determination of metal ions

The sensing phase was evaluated for the simultaneous determination of Cu(II), Hg(II) and Zn(II) in binary and ternary mixtures. The central composite design was employed to prepare the set of solutions in the concentration range from 2.50 to 50.0 μmol l^{-1}. This experimental design combines a complete fractional design of one or two levels, with additional points (star point) and at least one point in the centre of the design. This point is selected to provide an evaluation of the variance of the predicted response. It is an alternative to the full-factorial design, as it requires a lower number of experiments, keeping the quality of the results [39, 40].

The strategy adopted for the construction of the calibration models was based on the evaluation of emission spectra (420–650 nm) obtained with excitation wavelength set at 410 nm and along a reaction time of 10 min, acquired at time intervals of 2 min. A scanning rate of 120 nm min^{-1} was employed, as it provides emission spectra with better signal-to-noise ratio. All the calculation was performed with the relative I_0/I_i spectra, where I_0 refers to the reference spectrum and I_i stands for the spectrum at the time i, as the fluorescence signals obey the Stern–Volmer model. The I_0/I_i spectra were initially submitted to a pre-processing in order to minimise instrumental noises and baseline offset [41, 42]; smoothing procedures of moving average, median filter and Savitzky–Golay filter, all of the

Table 3 Results obtained for the prediction Cu(II) and Hg(II) concentrations in a binary mixture in aqueous phosphate buffer solution pH 5.0

Cu(II) (μmol l^{-1})[a]			Hg(II) (μmol l^{-1})[b]		
Expected	Predicted	Error (%)	Expected	Predicted	Error (%)
17.3	16.8	−2.9	5.16	5.41	4.8
17.3	17.0	−1.7	15.5	15.5	0.0
11.5	11.0	−4.3	3.06	3.18	3.9
3.39	3.68	8.6	10.3	10.2	−0.9
11.5	11.3	−1.7	23.7	24.0	1.3
34.6	34.7	0.3	31.0	30.8	−0.6

[a] From the I_0/I spectra; smoothing procedure: moving average (31-point window), 1,155 variables (time interval=2–10 min), three latent variables, RMSEP= 0.46 μmol l^{-1}

[b] From the I_0/I spectra; smoothing procedure: moving average (31-point window), 1,386 variables (time interval=0–10 min), three latent variables, RMSEP= 0.26 μmol l^{-1}

Table 4 Results of the prediction of the Cu(II) and Zn(II) concentrations in a binary mixture in aqueous phosphate buffer solution pH 5.0

Cu(II) (μmol l^{-1})[a]			Zn(II) (μmol l^{-1})[b]		
Expected	Predicted	Error (%)	Expected	Predicted	Error (%)
5.76	7.93	37.7	19.7	18.1	−8.1
11.5	12.6	9.6	11.5	11.5	0.0
11.5	12.2	6.1	5.76	6.25	8.5
23.0	23.4	1.7	15.0	17.0	13.3
28.8	28.3	−1.7	28.8	28.0	−2.8
34.6	35.4	2.3	26.5	24.5	−7.6

[a] From the I_0/I spectra; smoothing procedure: moving average (41-point window), 693 variables (time interval=6–10 min), two latent variables, RMSEP= 1.56 μmol l^{-1}

[b] From the I_0/I spectra; smoothing procedure: median filter (21-point window), 1,155 variables (time interval=2–10 min), three latent variables, RMSEP= 1.38 μmol l^{-1}

them based on different window sizes, were used. In addition, an exploratory analysis was performed, aimed at extracting information regarding the behaviour and the influence of the samples on the calibration models.

Models were constructed by employing PLS regression, as it is efficient to deal with experimental noise and data collinearity. In this regression, all the relevant variables are included in the model and the calibration can be adequately performed even in the presence of interfering species. PLS is based on latent variables, maximising the covariance between the fluorescence spectra (matrix **X**) and analyte concentrations (matrix **Y**). This approach is slightly different from PCR, which is based on principal components and maximises the variance on the matrix X for the direct regression against matrix Y [43]. The models for prediction were constructed by the cross-validation (leave-one-out) approach. This strategy consists of removing one sample of the calibration set and constructing a model in its absence. This sample is then tested as a validation sample of the prediction model. Such procedure is employed for all samples of the calibration set, allowing construction of the final model for this set of solutions [44].

The variability of the calibration set must represent the whole set of samples, including those for prediction. In order to improve the variability of the calibration set, different strategies have been described in the literature, such as the successive projection algorithm [45] and the Kennard–Stone algorithm [46]. In the latter algorithm, which was employed throughout this work, the first sample selected is the one that represents the highest distance from the mean sample; the second sample selected is the one that displays the highest distance from the first one, and so on.

The results shown in Tables 3, 4 and 5 (binary mixtures between Cu(II), Hg(II) and Zn(II)) and Table 6 (ternary mixture of these ions) were obtained from prediction models constructed with 20 calibration samples in the concentration range from 2.5 to 50 μmol l^{-1}. Different data pre-processing approaches were employed as indicated. The root mean square error of prediction (RMSEP) values obtained in all experiments are within the standard deviation of the measurement, demonstrating the robustness of the prediction model. As it can be noted, the results for prediction are in agreement with the expected values, as

Table 5 Results of the prediction of the Hg(II) and Zn(II) concentrations in a binary mixture in aqueous phosphate buffer solution pH 5.0

Hg(II) (μmol l^{-1})[a]			Zn(II) (μmol l^{-1})[b]		
Expected	Predicted	Error (%)	Expected	Predicted	Error (%)
10.3	10.1	−1.9	11.5	11.2	−2.6
5.16	4.84	−6.2	5.76	6.60	14.6
20.6	22.2	7.8	17.3	18.2	5.2
25.8	25.6	−0.8	28.8	27.0	−6.2
31.0	30.7	−1.0	17.3	16.6	−4.0

[a] From the I_0/I spectra; smoothing procedure: moving average (31-point window), 1,155 variables (time interval=2–10 min), two latent variables, RMSEP= 0.94 μmol l^{-1}

[b] From the I_0/I spectra; no smoothing procedure applied, 924 variables (time interval=4–10 min), two latent variables, RMSEP=3.32 μmol l^{-1}

Table 6 Results of the prediction of the Cu(II), Hg(II) and Zn(II) concentrations in a ternary mixture in aqueous phosphate buffer solution pH 5.0

Cu(II) (μmol l^{-1})[a]			Hg(II) (μmol l^{-1})[b]			Zn(II) (μmol l^{-1})[c]		
Expected	Predicted	Error (%)	Expected	Predicted	Error (%)	Expected	Predicted	Error (%)
11.9	13.9	16.8	12.9	14.6	13.2	14.4	16.3	13.2
19.0	18.2	−4.2	12.9	13.5	4.6	31.7	28.7	−9.5
26.1	27.1	3.8	28.4	27.2	−4.2	23.1	22.0	−4.8
26.0	27.0	3.8	28.3	29.9	5.6	40.3	38.4	−4.7

[a] From the I_0/I spectra; smoothing procedure: Savitzky–Golay filter (window size 35), 907 variables (time interval=4–10 min), two latent variables, RMSEP=1.14 μmol l^{-1}

[b] From the I_0/I spectra; smoothing procedure: median filter (window size 41), 693 variables (time interval=6–10 min), three latent variables, RMSEP=2.42 μmol l^{-1}

[c] From the I_0/I spectra; smoothing procedure: moving average (window size 41), 693 variables (time interval=6–10 min), two latent variables, RMSEP=2.14 μmol l^{-1}

they do not significantly differ at a confidence level of 95%. This fact demonstrates the robustness of the sensing phase, as leaching of the ligand, if it happened at all, did not affect the performance of the whole system.

Finally, the sensor was applied to the determination of these metal ions in spring waters in order to assess its analytical performance. As no waters with enough heavy metal ions contamination were available, commercial samples were spiked with different amounts of Cu(II) and Hg(II) and subject to analysis with the novel optosensor. The results collected in Table 7 demonstrate the analytical performance of the sensing phase for simultaneous determination of heavy metal ions in water. Comparing these results with those reported in the simultaneous determination of the analytes in *solution* [6], the performance of the BSOH optical sensor is evident, as the operational concentration ranges are similar and the measurement relative errors are of the same order of magnitude, with the advantage of automating the analyses with the sensing device.

Conclusions

The new engineered ligand based on a fluorescent bipyridine (BSOH) developed in this work interacts with different heavy metal ions. These interactions cause a static deactivation of the fluorescence signal, as indicated by the excited state lifetime of the indicator dye. Covalent immobilisation of BSOH in a sol-gel matrix preserved its fluorescent properties, and no leaching was observed from the solid. This characteristic allowed its application to the simultaneous determination of Cu(II), Hg(II) and Zn(II) in binary and ternary mixtures in water, providing results with low values of RMSEP and in agreement to the expected values, as demonstrated for the first time in the determination of Cu(II), Hg(II) and Zn(II) in mineral waters using multivariate calibration methods. Other luminescent indicator ligands are currently being explored in our laboratory to expand both the slate of metal ion determinants and the usability with different instrumentation, particularly the

Table 7 Results of the determinations of Cu(II) and Hg(II) in spring water samples spiked with these metal ions, using the BSOH optosensor

Cu(II) (μmol l^{-1})[a]			Hg(II) (μmol l^{-1})[b]		
Expected	Predicted	Error (%)	Expected	Predicted	Error (%)
14.3	13.4	−6.3	10.1	16.3	61.4
28.2	30.4	7.8	29.7	28.3	−4.7
4.89	7.96	62.8	15.1	14.4	−4.6
26.7	25.9	−3.0	28.3	27.1	−4.2

[a] From the I_0/I spectra; smoothing procedure: Savitzky–Golay filter (41-point window), 1,135 variables (time interval=2–10 min), three latent variables, RMSEP=4.09 μmol l^{-1}

[b] From the I_0/I spectra; smoothing procedure: Savitzky–Golay filter (41-point window), 1,135 variables (time interval=2–10 min), three latent variables, RMSEP=2.76 μmol l^{-1}

state-of-the-art one available nowadays for in situ optosensing of dissolved oxygen in waters.

Acknowledgments The authors thank Dr. Ana Castro for the synthesis of the BSOH ligand. Financial support from CAPES (CAPES/DGU 125/06), the Spanish Ministry of Education and Science (PHB2005-0030-PC, CTQ2009-14565-C03), FAPESP (05/04258-6) and CNPq/FAPESP (INCTAA) is gratefully acknowledged. This project has been partially funded by the Madrid Community Government (CM-S-505/AMB/0374) and UCM-Santander grant (GR58-08-910072).

References

1. Huang W, Cao L, Shan X, Xiao Z, Wang Q, Dou S (2010) Arch Environ Contam Toxicol 58:140–150
2. Sanches-Pedreño C, Ortuño JA, Albero MI, Garcia MI, Valero MV (2000) Anal Chim Acta 414:195–203
3. Serrano N, Díaz-Cruz JM, Ariño C, Esteban M (2010) Anal Bional Chem 396:1365–1369
4. Wolfbeis OS (2004) In: Narayanaswamy R, Wolfbeis OS (eds) Optical sensors: industrial, environmental and diagnostic applications. Springer, Berlin, pp 1–34
5. Jerónimo PCA, Araújo AN, Montenegro MCBSM (2004) Sens Actuators B 103:167–177
6. Mikami D, Ohki T, Yamaji K, Ishihara S, Cittero D, Hagiwara M, Suzuki K (2004) Anal Chem 76:5726–5733
7. Vaughan AA, Narayanaswamy R (1998) Sens Actuators B 51:368–376
8. Raimundo IM Jr, Narayanaswamy R (2003) Sens Actuators B 90:189–197
9. Ozturk G, Alp S, Ertekin K (2007) Dyes Pigm 72:150–156
10. Oter O, Ertekin K, Kilincarslan R, Ulusoy M, Cetinkaya B (2007) Dyes Pigm 74:730–735
11. Aksuner N, Henden E, Yilmaz I, Cukurovali A (2008) Sens Actuators B 134:510–515
12. Kalyan Y, Pandey AK, Bhagat PR, Acharya R, Natarajan V, Naidu GRK, Reddy AVR (2009) J Hazard Mater 166:377–382
13. Yari A, Afshari N (2006) Sens Actuators B 119:531–537
14. Chamjangali MA, Soltanpanah S, Goudarzi N (2009) Sens Actuators B 138:251–256
15. Scindia YM, Pandey AK, Reddy AVR, Manohar SB (2004) Anal Chim Acta 515:311–321
16. Madden JE, Cardwell TJ, Cattrall RW, Deady LW (1996) Anal Chim Acta 319:129–134
17. Ma QJ, Zhang XB, Zhao XH, Gong YJ, Tang J, Shen GL, Yu RQ (2009) Spectrochim Acta A 73:687–693
18. Lee BS, Lee JE, Seo L, Jeong IY, Lee SS, Jung JH (2007) Adv Funct Mater 17:3441–3446
19. Plaschke M, Czolk R, Ache HJ (1995) Anal Chim Acta 304:107–113
20. Delmarre D, Méallet R, Bied-Charreton C, Pansu RB (1999) J Photochem Photobiol A Chem 124:23–28
21. Jerónimo PCA, Araújo AN, Montenegro MCBSM (2007) Talanta 72:13–27
22. Yang X, Wang J, Wang L (2009) Opt Commun 282:2502–2505
23. Lukowiak A, Strek W (2009) J Sol-Gel Technol 50:201–215
24. Carmona N, Herrero-Hernades E, Llopis J, Villegas A (2008) J Sol-Gel Technol 47:31–37
25. Aksuner A, Henden E, Yilmaz I, Cukurovali A (2009) Dyes Pigm 83:211–217
26. Mikata Y, Yamanaka A, Yamashita A, Yano S (2008) Inorg Chem 47:7295–7301
27. Salman H, Tal S, Chuvilov Y, Solovey O, Abrahan Y, Kapon M, Suwinska K, Eichen Y (2006) Inorg Chem 45:5315–5320
28. Praveen L, Ganga VB, Thirumalai R, Sreeja T, Reddy MLP, Varma RL (2007) Inorg Chem 46:6277–6282
29. Saleh N (2009) Luminescence 24:30–34
30. Núñez C, Bastida R, Macías A, Bértolo E, Fernandes L, Capelo JL, Lodeiro C (2009) Tetrahedron 65:6179–6188
31. He G, Zhao Y, He C, Liu Y, Duan C (2008) Inorg Chem 47:5169–5176
32. Samadi-Maybodi A, Darzi SKHN (2008) Spectrochim Acta A 70:1167–1172
33. Al-Degas YS, Al-Ghouti MA, El-Sheikh AH (2009) J Hazard Mater 169:128–135
34. Ensafi AA, Khayamian T, Benvidi A, Mirmomtaz E (2006) Anal Chim Acta 561:225–232
35. Afkhami A, Abbasi-Tarighat A, Khanmohammadi H (2009) Talanta 77:995–1001
36. Schilt AA (1969) Analytical applications of 1,10-phenanthroline and related compounds. Pergamon, Oxford
37. McBryde WAE (1977) Critical review of equilibrium data for proton and metal complexes of 1, 10-phenanthroline, 2, 2′-bipyridyl and related compounds: stability constants of metal complexes Part A: critical evaluation of equilibrium constants in solution (IUPAC Publications). Elsevier, The Netherlands
38. Likhtenshtein G (2010) Stilbenes. Applications in chemistry, life sciences and materials science. Wiley, New York
39. Tarley CRT, Silveira G, Matos WNL, Silva GD, Bezerra EGP, Miro M, Ferreira SLC (2009) Microchem J 92:58–67
40. Barros Neto B, Scarmino IS, Bruns RE (2003) Como fazer experimentos. Unicamp, Campinas
41. Ferreira MMC, Antunes AM, Melgo MS, Volpe PLO (1999) Quim Nova 22:724–731
42. Massart DL, Vandeginste BGM, Buydens SJ, Lewi PJ, Smeyers-Verbeke J (1997) Handbook of chemometrics and qualimetrics: part B. Elsevier, Amsterdam
43. Cunha AP JR, Cunha VPP, Silveira L Jr, Martin AA (2003) Quim Nova 26:850–854
44. Reche RV, Franco DW (2009) Quim Nova 32:332–336
45. Filho HAD, Galvao RKH, Araújo MCU, Silva EC, Saldanha TCB, Jose GE, Pasquini C, Raimundo IM Jr, Rohwedder JJR (2004) Chemom Intell Lab Syst 72:83–91
46. Kennard RW, Stone LA (1969) Technometrics 11:137–148